Study of $N = 50$ gap evolution around $Z = 32$: new structure information for ^{82}Ge

D Thisse, M Lebois, D Verney, J.N Wilson, N Jovančević, M Rudigier, R Canavan, D Etasse, P Adsley, A Algora, et al.

Study of $N = 50$ gap evolution around $Z = 32$: New structure information for ^{82}Ge

D. Thisse[1a], M. Lebois[1,2], D. Verney[1], J. N. Wilson[1], N. Jovančević[3], M. Rudigier[4,5], R. Canavan[4,6], D. Etasse[7], P. Adsley[1], A. Algora[9], M. Babo[1], K. Belvedere[4], J. Benito[10], G. Benzoni[11], A. Blazhev[12], A. Boso[6], S. Bottoni[11,13], M. Bunce[6], R. Chakma[1], N. Cieplicka-Oryńczak[14], S. Courtin[15,16], M. L. Cortés[17], P. Davies[18], C. Delafosse[1], M. Fallot[19], B. Fornal[14], L. Fraile[10], D. Gjestvang[20], A. Gottardo[21], V. Guadilla[9], R.-B. Gerst[12], G. Häfner[1,12], K. Hauschild[1], M. Heine[15], C. Henrich[5], I. Homm[5], J. Hommet[7], F. Ibrahim[1], Ł. W. Iskra[11,14], P. Ivanov[6], S. Jazrawi[4,6], A. Korgul[8], P. Koseoglou[5,22], T. Kröll[5], T. Kurtukian-Nieto[23], L. Le Meur[19], S. Leoni[11,13], J. Ljungvall[1], A. Lopez-Martens[1], R. Lozeva[1], I. Matea[1], K. Miernik[8], J. Nemer[1], S. Oberstedt[24], W. Paulsen[20], M. Piersa -Silkowska[8], W. Poklepa[8], Y. Popovitch[1], C. Porzio[11,13,25], L. Qi[1], D. Ralet[26], P. H. Regan[4,6], D. Reygadas-Tello[27], K. Rezynkina[28], V. Sánchez-Tembleque[10], S. Siem[20], C. Schmitt[15], P.-A. Söderström[5,29], K. Solak[8], C. Sürder[5], G. Tocabens[1], V. Vedia[10], N. Warr[12], B. Wasilewska[14], J. Wiederhold[5], M. Yavahchova[30], F. Zeiser[20], and S. Ziliani[11,13]

[1] Université Paris-Saclay, CNRS/IN2P3, IJCLab, 91405 Orsay, France
[2] Institut Universitaire de France, 1 Rue Descartes, 75005 Paris, France
[3] Department of Physics, Faculty of Science, University of Novi Sad, Trg Dositeja Obradovica 3, 21000 Novi Sad, Serbia
[4] School of Mathematics and Physics, University of Surrey, Guildford, GU2 7XH, United Kingdom
[5] Institut für Kernphysik, Technische Universität Darmstadt, 64289 Darmstadt, Germany
[6] National Physical Laboratory, Teddington, Middlesex TW11 0LW, United Kingdom
[7] Normandie Univ, ENSICAEN, UNICAEN, CNRS/IN2P3, LPC Caen, 14000 Caen, France
[8] Faculty of Physics, University of Warsaw, Warsaw, Poland
[9] Instituto de Física Corpuscular, CSIC-University of Valencia, Valencia, Spain
[10] Grupo de Física Nuclear and IPARCOS, Universidad Complutense de Madrid, Madrid, Spain
[11] Istituto Nazionale di Fisica Nucleare, Sezione di Milano, Via Celoria 16, 20133 Milano, Italy
[12] Institut für Kernphysik, Universität zu Köln, 50937 Köln, Germany
[13] Dipartimento di Fisica, Universitá degli Studi di Milano, Via Celoria 16, 20133 Milano, Italy
[14] Institute of Nuclear Physics, Polish Academy of Sciences, PL-31342 Krakow, Poland
[15] Institut Pluridisciplinaire Hubert Curien, 23 rue du Loess, 67037 Strasbourg, France
[16] CNRS, UMR7178, 67037 Strasbourg, France
[17] RIKEN Nishina Center, 2-1 Hirosawa, Wako, Saitama 351-0198, Japan
[18] School of Physics and Astronomy, University of Manchester, Oxford Road, Manchester M13 9PL, United Kingdom
[19] Subatech, IMT-Atlantique, Université de Nantes, CNRS-IN2P3, F-44307 Nantes, France
[20] University of Oslo, Departement of Physics, P.O. Box 1048, Blindern, 0316 Oslo, Norway
[21] INFN Laboratori Nazionali di Legnaro, Viale dell'Universitá, 2, I-35020 Legnaro, Italy
[22] GSI Helmholtzzentrum für Schwerionenforschung GmbH, Planckstr.1, 64291 Darmstadt, Germany
[23] CENBG, UMR5797, Université de Bordeaux, CNRS, F-33170 Gradignan, France
[24] European Commission, Joint Research Center, 2440 Geel, Belgium
[25] TRIUMF, 4004 Wesbrook Mall, Vancouver, BC V6T 2A3, Canada
[26] Grand Accélérateur National d'Ions Lourds, Bd Henri Becquerel, 14076 Caen, France
[27] School of Computing, Engineering and Mathematics, University of Brighton, Brighton, BN2 4GJ, United Kingdom
[28] Institute for Nuclear and Radiation Physics, KU Leuven, 3000 Leuven, Belgium
[29] Extreme Light Infrastructure-Nuclear Physics (ELI-NP)/Horia Hulubei National Institute for Physics and Nuclear Engineering (IFIN-HH), Str. Reactorului 30, Bucharest-Măgurele 077125, Romania
[30] Institute for Nuclear Research and Nuclear Energy, Bulgarian Academy of Sciences, 1784 Sofia, Bulgaria

Received: date / Revised version: date

Abstract. Medium spin states of light N=50 isotones have been populated using fast neutron-induced fission of ^{232}Th. Online prompt γ spectroscopy has been performed using the hybrid γ spectrometer ν-Ball coupled to the LICORNE directional neutron source at the ALTO facility of IJCLab. Medium spin states of the neutron-rich nucleus ^{82}Ge have been investigated using γ-γ and γ-γ-γ coincidence data to exploit the resolving power of ν-Ball. Two new transitions were assigned to this nucleus and a new level was placed in the level scheme. We tentatively assigned to this new state a (7^+) spin-parity, which is interpreted as a new $N = 50$ core breaking state. This provides further insight into the energy evolution of the $N = 50$ shell gap toward ^{78}Ni.

1 Introduction

Since the pioneering work of Engelmann *et al.* [1] a considerable experimental effort has been devoted to probe the doubly magic nature of ^{78}Ni. It is only recently that excited states of ^{78}Ni could be populated for the first time in an experiment performed at RIKEN [2]. One of these states, considered as its first 2^+ level, decays by a 2.6 MeV γ transition, a sufficiently high enough energy to indicate the doubly magic nature of this nucleus. This suggests that the shell closure associated with the $N = 50$ magic number remains robust down to $Z = 28$. Nevertheless, the evolution of the single-particle gap size from β stability towards the exotic ^{78}Ni, at the origin of the magic nature of the $N = 50$ isotones, is still poorly understood. Indeed, it is apparent from both mass [3,4] and spectroscopic [5, 6,7,8,9,10] data that the size of the effective $N = 50$ gap continuously decreases from stability down to $Z = 32$. This reduction must certainly be followed by a stabilization around $Z = 30$, a phenomenon that has still not received any theoretical explanation.

Extracting a pure single-particle (monopole) gap and its evolution from experimental data is a particularly difficult task as soon as one moves away from the anchor points constituted by clearly doubly magic nuclei. Fortunately, in this particular mass region, an interesting and remarkable correlation between both mass and spectroscopic data has been highlighted [11], and more recently further exploited by Dudouet *et al.* [10]. Hence by combining the observables from these very different types of measurements it is possible to study the $N = 50$ gap evolution in precise detail.

The objective of this work is to enhance the available body of spectroscopic data on states carrying information on the size of the $N = 50$ energy gap for the nucleus ^{82}Ge. Near $Z = 32$ this gap is located between the two neutron single-particle (sp) orbitals $\nu 1g_{9/2}$ and $\nu 2d_{5/2}$. The states of interest belong to a multiplet of six levels with total angular momentum ranging from 2^+ to 7^+ associated to the $N = 50$ core-breaking particle-hole $(\nu 1g_{9/2})^{-1}(\nu 2d_{5/2})^1$ configuration. The most interesting members of this multiplet are at the highest spins because they are the least subject to configuration mixing and, consequently, the least sensitive to correlations of various origins (mainly quadrupole). For instance, between $Z = 28$ and 40 the protons fill the $(\pi 1f_{5/2})(\pi 2p_{3/2})(\pi 2p_{1/2})$ sp-orbitals. With 4 protons, it is not possible to produce an angular momentum higher than $6\hbar$ with any accessible configuration of this valence space. Therefore, the yrast 7^+ state of ^{82}Ge should be the first level whose energy is almost "cleanly" characteristic of the size of the neutron shell gap.
Populating medium-spin yrast states of very neutron-rich nuclei is notoriously challenging. Gamma-ray spectroscopy of fission fragments is one of the best technique to perform this kind of study [12]. Available information on such states in ^{82}Ge mainly originates from spontaneous fission of $^{248}_{96}$Cm [7] and $^{252}_{98}$Cf [8] but must be incomplete as no obvious candidate for the 7^+ state has been identified so far. In order to complement this spectroscopy we have exploited the fast neutron-induced fission of ^{232}Th in an experiment performed at the ALTO facility of IJCLab using the ν-Ball γ ray spectrometer [13]. In the present work we report on this experiment and its results. In the following sections a description of the experimental setup will be presented along with the methods used to process and reconstruct the γ coincidence data. The level scheme construction methodology is then validated on the better known case of ^{84}Se, the closest even-even $N = 50$ neighbor of ^{82}Ge. The application of this analysis method to the case of ^{82}Ge allows us to add to its yrast/near-yrast level scheme a new state and two previously unknown transitions. The structure of this new state is then discussed by considering both experimental systematic and shell-model phenomenological arguments.

[a] *Present address:* damien.thisse@cea.fr

2 Presentation of the experimental setup

During a period of over a year the ν-Ball [14] γ spectroscopy experimental campaign was performed at the ALTO facility of IJCLab in Orsay. One of the experiments involved the study of neutron-rich nuclei produced by the fast neutron-induced fission of ^{232}Th.

2.1 Description of the ν-Ball spectrometer

The ν-Ball array was composed of 24 HPGe Clover detectors from the GAMMAPOOL [15], 9 co-axial HPGe from the UK-French LOANPOOL [16], and 20 $LaBr_3$ from the FATIMA [17] and UKNDN [18] collaborations. Detailed information about the positioning of the detectors can be found in [13]. An energy resolution of 2.5 keV at 1.33 MeV and a time resolution of about 12 ns were achieved for the HPGe part of the array.

The photopeak efficiency of the latter was 4.3(2) % for a 1.3 MeV γ-ray. However, the use of massive targets (129 g of metallic ^{232}Th), necessary to achieve high fission rates, had a significant impact on the low-energy detection efficiency. Figure 1 shows the absolute efficiencies of the HPGe part of the array measured with a point-like calibrated source of ^{152}Eu (dotted line) and with the intrinsic activity of the ^{nat}Th target (dashed line). The difference is visible in the low energy region (below 700 keV), where the absorption by the target induces a considerable decrease of the efficiency. Finally, the ν-Ball array used a fully digital data acquisition system named FASTER [19] and developed at the Laboratoire de Physique Corpusculaire (LPC) in Caen, France.

2.2 Description of the neutron beam and ^{nat}Th target

The fission of ^{232}Th was induced by the fast-neutron beam produced with the LICORNE neutron source [20]. A primary 80 nA pulsed ^{7}Li beam produced using the 15 MV Tandem accelerator of the ALTO facility impinged on a gaseous hydrogen cell of 3.5 cm length. A cone-shaped

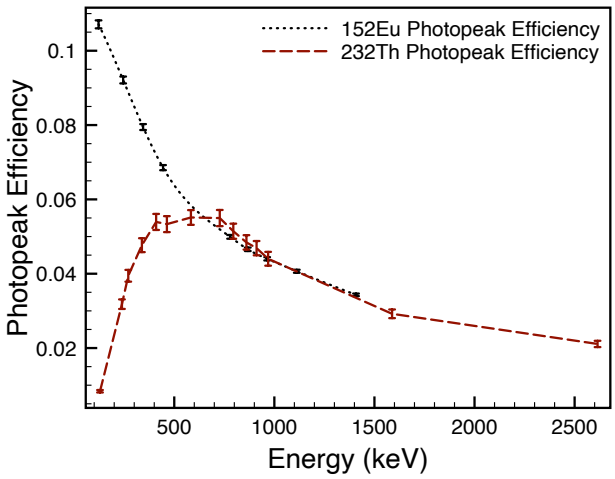

Fig. 1: Measured absolute photopeak efficiency of the Germanium detectors of the ν-Ball array. The dotted black curve corresponds to the efficiency measured with a calibrated point-like source of ^{152}Eu. The dashed red line corresponds to the absolute efficiency measured with the massive target of ^{nat}Th. We observe that in the second case, the efficiency for the low energy γ-rays, below 700 keV, is lower because of the absorption in the target.

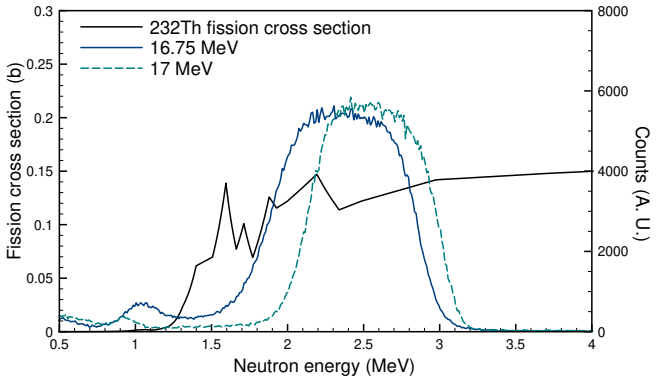

Fig. 2: The black continuous line represents the fission cross-section of $^{232}_{90}$Th, given in barns on the left Y-axis, as a function of the incident neutron energy [21]. The two dashed curves represent the energy distribution of the neutrons produced with LICORNE for two incident ^{7}Li beam energies and measured in a liquid scintillator placed at 3 meters from the source. These spectra were obtained online and are not corrected for neutron detection efficiency. For comparison purposes, the two spectra have been normalized and an arbitrary count rate for these two curves is given by the right Y-axis.

secondary beam of neutrons was emitted by the reaction p(^{7}Li, n)^{7}Be in inverse kinematics. The opening angle of the cone becomes larger as the energy of the primary ^{7}Li beam increases. The incident primary beam energy was set to maximize the cross-section over the neutron energy range, as shown on Figure 2. However, the neutron cone opening angle had also to be limited to less than 25 degrees to avoid neutrons hitting the $LaBr_3$ detectors directly. Hence, the optimal primary beam energy was determined to be 16.75 MeV.

The ^{7}Li beam was bunched with a 2 ns pulse width and a 2.5 MHz repetition rate. This time structure provides additional information which can help to identify fission events. The timestamps of the radio-frequency (RF) signal used to bunch the beam were sent to the data acquisition system at a scaled down rate in order to determine γ-ray arrival times relative to the beam pulsation.

The resulting 2.3 MeV average energy beam of neutrons bombarded a 129 g ^{nat}Th target, mainly composed of ^{232}Th, placed at the center of the spectrometer. The target was made of eight 1 mm thick disks of ^{nat}Th of varying diameters placed 1 cm apart, encapsulated in a thin aluminium container with a conical shape that matched the profile of the neutron beam. The effective density was 0.984 g/cm^3, needed to minimise the loss of efficiency for low-energy γ-rays. The choice of ^{232}Th was mainly motivated by higher fission yields [21] in the ^{78}Ni mass region compared to other fissioning systems. The fission rate during the experiment was estimated at 25(5) kHz, which has to be compared with the 5.2 MBq intrinsic activity of the ^{nat}Th target. Thus several gating conditions were needed to select fission from intrinsic decays and other background events with low multiplicity. These will be presented in the next section.

3 ^{232}Th(n,f) experiment data analysis

Before reconstructing fission events, a preliminary data treatment has been performed such as: energy calibration, time alignment, *etc.* Detailed information about these procedures can be found in [22]. In the following, we decided to focus on providing all the necessary details about fission reaction selection.

One of the key parameters needed to reconstruct the fission events is the time structure of the neutron beam. The RF pulsation signal is sent to the datastream and fission events should be found in a short time window around these prompt beam bursts. Events were built with a length equivalent to the beam pulsation period (400 ns), and starting 60 ns before the beam RF signal. This time shift was used to get a better estimation of the uncorrelated background since it can be defined in a short pre-prompt time window before the beam pulse. A set of gating conditions that permits identification of fission from among all the contaminating reactions and decays has to be chosen. The latter were: the intrinsic activity of the target, (n,n') and (n,γ) reactions, p(^{7}Li,^{7}Li*)p' or Coulomb excitation (Coulex) reactions in LICORNE gas cell metallic structure, β-decay of fission fragments, *etc.* Fission and parasitic reactions emit γ-rays in the same energy range, from hundreds of keV to several MeV. On the other hand, fission events are usually characterized by a high γ-ray multiplicity ($\sim 8\,\gamma$ for $^{252}_{98}$Cf spontaneous fission), whereas other reactions and decays have lower multiplicities ($\sim 3\,\gamma$

for fragment β-decay or within the decay chain of ^{nat}Th). As mentioned in section 2, the intrinsic activity of the ^{nat}Th target is around 100 times higher than the fission rate. Assuming a Poisson distribution, one finds that there is an 86% of chance that at least one isotope of the ^{232}Th chain decays in a 400 ns time window. This probability is reduced to 22% in a 50 ns time window. Moreover, the share of beam pulses inducing a fission is estimated at 1%. Compiling all these values leads to a maximum of 0.14% of the pulses giving a pure fission event without contaminant pile-up, revealing the difficulty of perfectly selecting them.

Figure 3 shows two matrices representing the time difference between a detector signal and the corresponding beam pulsation signal on X-axis, and the energy deposited in the detector on the Y-axis in a part of the 400 ns pulse window. The top spectrum is for all the HPGe detectors, and the bottom one is for all the $LaBr_3$ detectors. The contour used to define the prompt region (*i.e.* in coincidence with the beam pulsing) is drawn on each diagram. More precisely, this contour was defined to be a 2σ selection of the gaussian time distribution at a given energy. It will be referred as the "prompt time window" in the fission event selection.

Since the objective is to build double or triple prompt γ coincidences that will give a unique signature to recognize fission fragments, a trigger based on event multiplicity was observed to be sufficient to get rid of a large fraction of the non-fission events. The least restrictive condition that can be applied in order to build a cube is to have at least 3 HPGe detectors hit, after add-back and Compton suppression (C3), in a one period pulse window. Then, since γ rays from the fission are emitted mainly in the prompt time window, a condition on the modular prompt (MP) multiplicity can further be applied to clean the spectra. A module corresponds to a $LaBr_3$ scintillator, or to the couple formed by a HPGe detector and its BGO.

The total projections of the triple γ cubes for several prompt multiplicity (3 to 5) conditions are shown on Figure 4. To characterize the quality of a selection condition, the γ-ray intensity at 376 keV from the most produced fission fragment ^{140}Xe was used. With no other condition on the modular prompt multiplicity, the integral for this peak is 3.94×10^6 counts. The peak-to-total (P/T) ratio evaluated in a 4σ energy window around the peak is 3.76(3) %. Adding a modular prompt multiplicity condition of at least 4 leads to an integral of 2.66×10^6 and a P/T ratio of 5.2(1) %. For a modular prompt multiplicity of at least 5 one obtains an integral of 1.21×10^6 and a P/T ratio of 6.4(3) %. Obviously, the higher this condition, the lower the background, but at the same time, the statistics for fission drop significantly, which unavoidably reduces the sensitivity of the measurement to the most weakly populated, and hence most exotic, fission fragments.

No condition on the total energy has been used as the superposition of high rate contaminating reactions may lead to a total energy close to those released in fission. It is also important to note that high multiplicity conditions may decrease the visibility of fission fragments emitting short γ cascades. Thus, several selection conditions may be used depending on the nucleus to be studied.

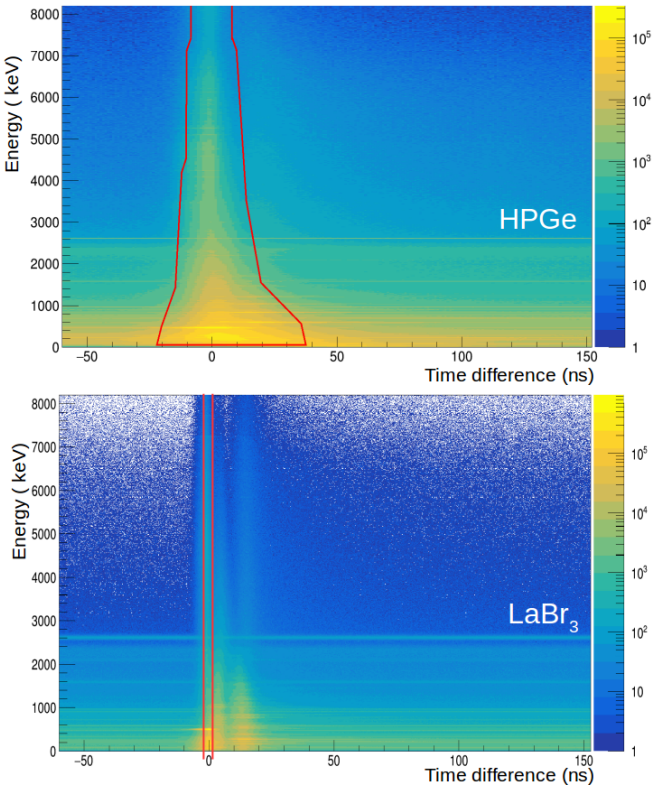

Fig. 3: Matrices representing the energy with respect to the time difference between a hit in a detector and the corresponding beam pulsation signal. The top spectrum is for all the HPGe detectors, the bottom one is for all $LaBr_3$ scintillators. In the latter, one sees the inelastic scattering of neutrons on $LaBr_3$ crystals around 15 ns. The prompt window for both type of detectors in drawn on each graph.

Once the trigger condition is passed, all the hits are grouped together into the same "fission event". Finally, the coincidences between γ-rays are reconstructed for the selected events and used to build prompt γ-γ matrices and γ-γ-γ cubes.

4 Results

The results presented in this section were obtained from the exploitation of the γ-γ-γ cube constructed using a C3MP4 condition (*i. e.* at least 4 modules hit in the prompt time window). The top spectrum (A) of Figures 5 and 6 shows the total projection of this cube. The dominant structures visible in the histograms are indicated with their origins. They were mainly produced by the (p,p') reactions in the gas cell in the $470-510$ keV region, by β-decay in the decay chain of $^{232}_{90}$Th, and by (n,n') reactions in the germanium crystals. As a matter of comparison, the most intense transition coming from fission ($2^+ \rightarrow 0^+$ of the most produced fission fragment ^{140}Xe) is indicated.

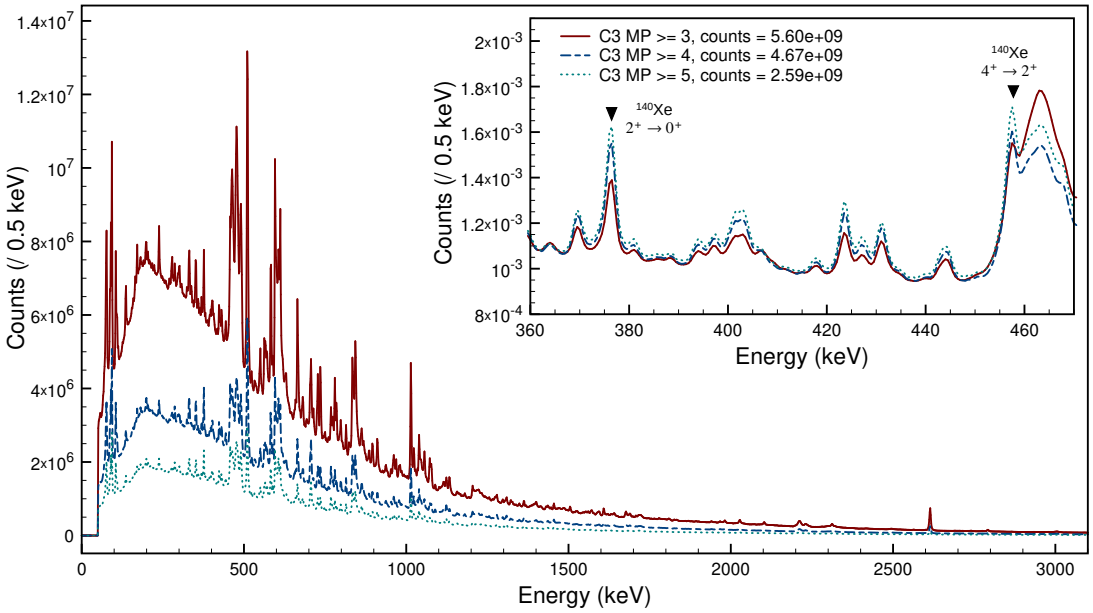

Fig. 4: Projection of the triple prompt γ cube for different trigger conditions. X-axis represents the energy, and the Y-axis is the number of counts per 0.5 keV. It shows that the higher the requested prompt modular multiplicity, the lower the background. The inset presents the same projections but normalized to the total integral. One clearly sees the improvement of the peak to background ratio for the transitions of ^{140}Xe at 376.7 and 457.6 keV.

4.1 Study of ^{84}Se

As a first step, the principle of our analysis was tested using the known $N = 50$ isotone ^{84}Se, the even-even neighbor to our nucleus of interest. The medium-spin states (with $I \leq 7$), likely to carry significant $N = 50$ core-breaking components, have previously been identified [5].

This test is essential to verify whether the reaction mechanism chosen in the present experiment does actually populate these states. A gate is applied on the $2^+ \rightarrow 0^+$ transition at 1454.5 keV [23] to see its coincidence spectrum, shown in part B of Figure 5. The most intense peaks, identified as transitions from the fission partners ^{146}Ba, are indicated. Moreover four transitions previously identified in coincidence with the $2^+ \rightarrow 0^+$ in ^{84}Se are also easily visible and listed in Table 1. The spectrum C of Figure 5 results from the double gate on both 1454.5 and 667.0 keV transitions ($4^+ \rightarrow 2^+$ and $2^+ \rightarrow 0^+$) further confirming the transition placements from previous work. Two other transitions from ^{84}Se are also visible. The level scheme resulting from our data analysis is presented in Figure 7 from which one can conclude that the chosen reaction mechanism is not only very selective in populating yrast states, but also suitable to reach angular momenta as high as $7\hbar$.

4.2 Study of ^{82}Ge

Given the previous results, we can now address the case of ^{82}Ge, and use the same starting point by applying a gate on the $2^+ \rightarrow 0^+$ transition at 1348.5 keV [24]. This results in spectrum B of Figure 6 where peaks at 646.1 and 1176.6 keV along with a doublet at 938.6, 940.5 keV, all well established transitions in ^{82}Ge [7,8], are clearly visible. Four γ-ray energies identified in the fission partner ^{148}Ce level scheme at 295.1, 386.2, 450.8 and 500.8 keV, and two from ^{150}Ce level scheme at 208.7 and 300.7 keV are also present in this spectrum. The following levels are confirmed in ^{82}Ge level scheme by the study of the set of all possible gated spectra: 1348.5-, 2287.1-, 2525.1-, 2933.2-, 3227.6 keV. It is worth noting that none of the transitions de-exciting the non yrast bands introduced by Hwang *et al.* [8] could be observed in our experiment.

A previously unreported γ ray at 720.3 keV in the 1348.5 keV gated data is visible in spectrum B of Figure 6. It does not correspond to any transitions in the partners nor to any possible transition between two known levels of ^{82}Ge. Spectrum E of Figure 6 contains γ events double-gated on the 1348.5 and 720.3 keV lines which clearly exhibit a peak centered around 939.4 keV. Its full width at half maximum (FWHM) of 5.7 keV, around twice the one of a single peak ($\sim$ 2.6 keV) in this energy region, leads to assume that it corresponds to the 938.6-, 940.5 keV doublet. Thus, we propose the existence of a new state at 3947.9 keV that decays solely to the state at 3227.6 keV.

Moreover, an additional transition at 294.1 keV has been identified. This transition is also observed in coincidences with both 1348.5 and 646.1 keV transitions as shown on Spectra C and D of Figure 6, along with the transition at 938.6 keV. Despite the small energy difference with a transition from the partner ^{148}Ce, $4^+ \rightarrow 2^+$ at 295.1 keV, no other transitions from the latter is observed in the gated spectrum – including the $2^+ \rightarrow 0^+$ at 158.5 keV. Additionally, this energy corresponds exactly to the dif-

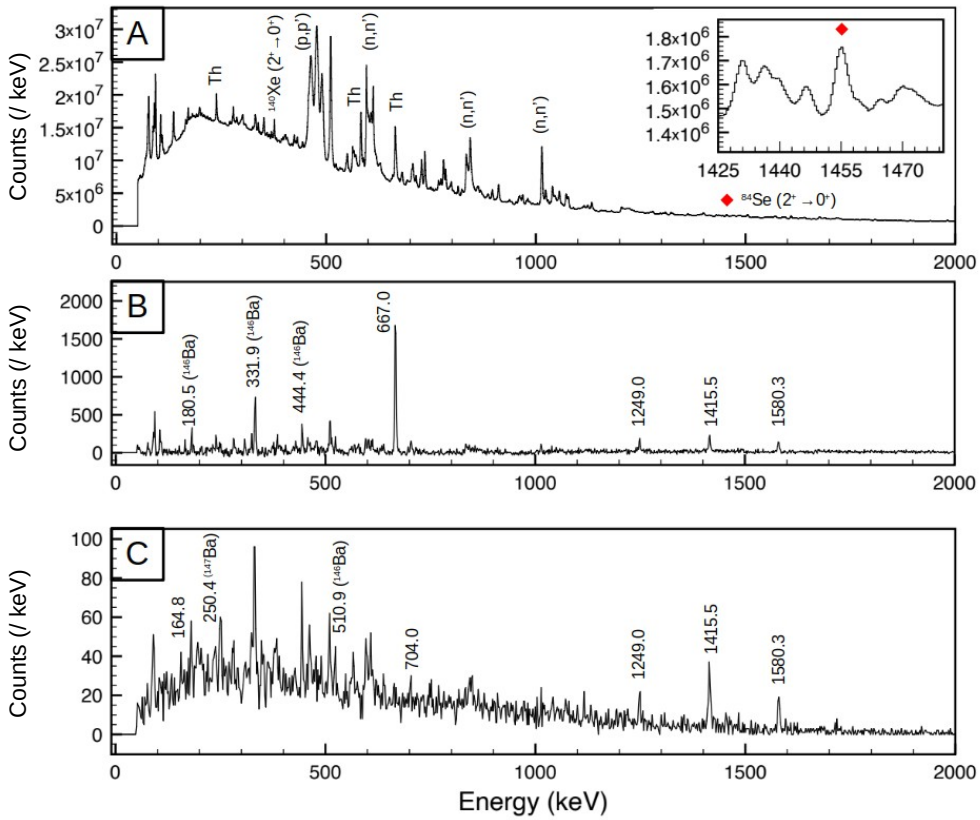

Fig. 5: Spectrum a: Total projection of the triple γ cube produced by the trigger C3MP4. The origins of principal peaks and structures are indicated. Th stands for the decay of the elements in the ^{nat}Th target, (n, n') for the inelastic diffusion of the neutrons from LICORNE and the fission, and (p, p') is for the inelastic diffusion of lithium on hydrogen in the LICORNE chamber. The transition $2^+ \rightarrow 0^+$ of the most produced fission fragment ^{140}Xe and of ^{84}Se are indicated for intensity comparison. Spectrum b: Spectrum gated on the 1455.1 keV transition of ^{84}Se. The peaks corresponding to transitions identified in a fission partner are indicated with the corresponding partner in brackets. Spectrum c: Spectrum double gated on both 1455.1 and 667.0 keV transitions.

ference between the levels at 3227.6 keV and 2933.2 keV. We therefore propose to attribute this previously unreported 294.1 keV line to a transition connecting these two excited states of ^{82}Ge. Table 2 summarizes all the levels and transitions observed in this work. The new level scheme resulting from our study is presented in Figure 7. Based on this new information, a discussion about the nuclear structure of ^{82}Ge and spin assignments is presented in the following section.

5 Discussion

5.1 Spin-parity assignments

As discussed above, our data allows the placement of two additional energy transitions and one additional excited state at 3947.9 keV in the level scheme of ^{82}Ge. We will examine the consequences of these placements on previous spin-parity assignments to some of the ^{82}Ge levels, and will propose one for the newly introduced state.

5.1.1 The new transition at 294.1 keV

A new decay branch has been found from the state at 3227.6 keV excitation energy to the 2933.2 keV state. The first was proposed as a (6^+), and the second as a (5^+) by Sahin *et al.* [9]. This makes the decay pattern of this 3227.6 keV state of ^{82}Ge very similar to that of the excited 6^+ state of the $N = 50$ isotone ^{84}Se, located at 3702.4 keV (see Figure 7). For ^{84}Se, the 6^+ nature of the latter is firmly established, as is the 5^+ nature of the state to which it decays via a low-energy 164.8 keV transition. The existence of the 294.1 keV transition therefore strengthens the spin-parity hypotheses (5^+) and (6^+) made by Sahin *et al.* for the 3227.6 keV and 2933.2 keV excited states of ^{82}Ge, respectively.

5.1.2 The case of the 2525.1 keV state

The excited state of ^{82}Ge placed at 2521(2) keV excitation energy by Sahin *et al.* [9] and at 2524.7(4) keV by

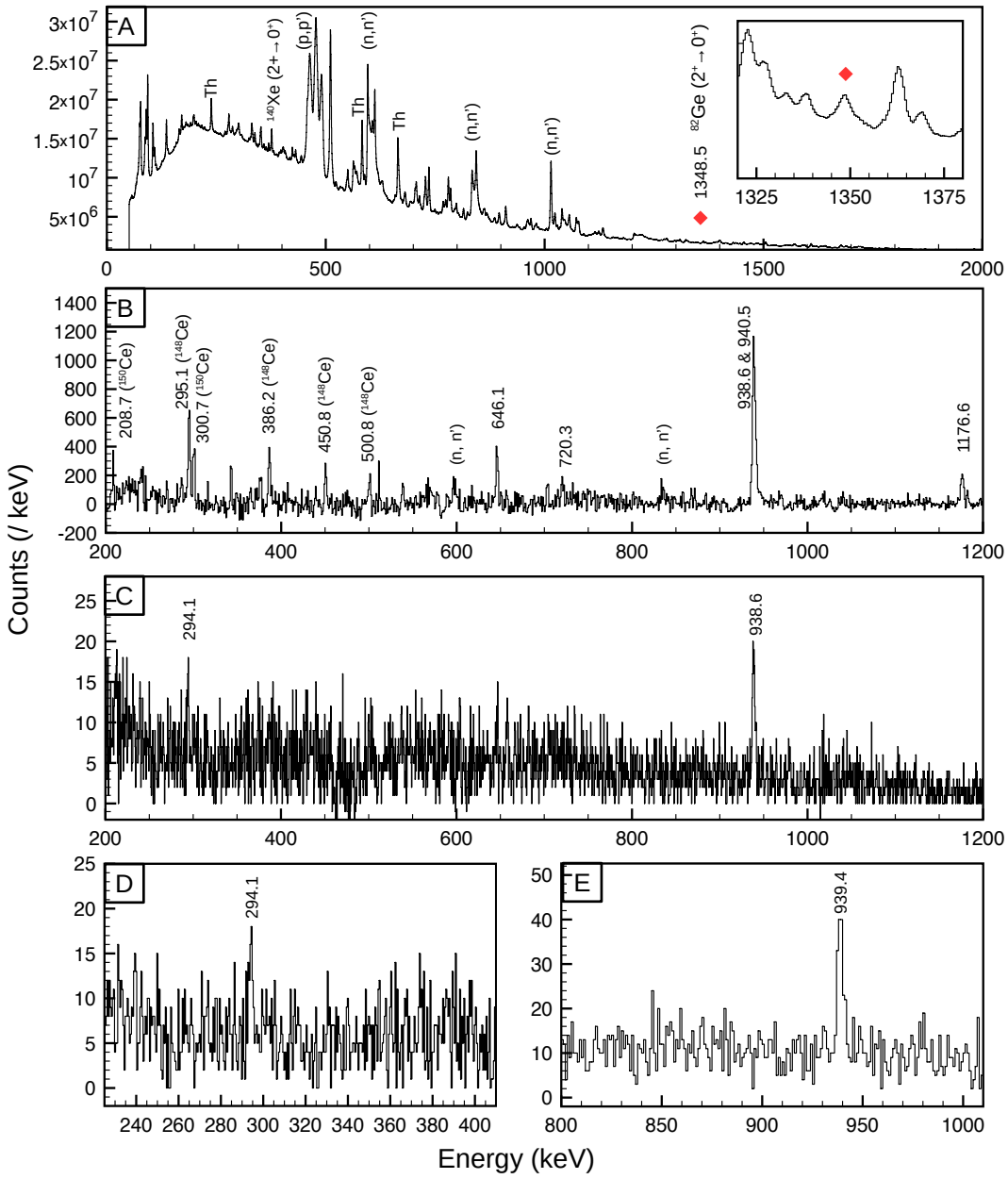

Fig. 6: Spectrum a: Same as in Figure 5, but this time, the $2^+ \rightarrow 0^+$ transition of ^{140}Xe is compared to the corresponding transition in ^{82}Ge. Spectrum b: Spectrum gated on the 1348.5 keV transition of ^{82}Ge. Ten identified transitions are indicated. Four of them are coming from the fission partner ^{148}Ce, and two from ^{150}Ce. Spectrum c: Spectrum double gated on both 1348.5 and 646.1 keV transitions. Two peaks are observed in coincidence at 938.6 keV and 294.1 keV. Spectrum d: Zoom on the low energy region from the Spectrum c to give a better insight on the 294.1 keV transition. Spectrum e: Spectrum double gated on both 1348.5 and 720.3 keV transitions. A structure is observed at 939.4 keV.

Level Energy (keV)		J^π	$J_i^\pi \rightarrow J_f^\pi$	E_γ (keV)	
This work	Literature			This work	Literature
1455.1(1)	1454.55(8)	2^+	$2^+ \rightarrow 0^+$	1455.1(1)	1454.66
2122.1(2)	2121.65(10)	4^+	$4^+ \rightarrow 2^+$	667.0(1)	666.99
3371.1(3)	3370.54(16)	(6^+)	$(6^+) \rightarrow 4^+$	1249.0(1)	1248.88
3537.6(3)	3537.09(18)	(5^+)	$(5^+) \rightarrow 4^+$	1415.5(1)	1415.30
3702.4(4)	3701.47(19)	(6^+)	$(6^+) \rightarrow 4^+$	1580.3(2)	1580.00
			$(6^+) \rightarrow (5^+)$	164.8(1)	164.18
4407.1(6)	4405.8(3)	(7^+)	$(7^+) \rightarrow 6^+$	704.0(2)	704.34

Table 1: List of all the levels of ^{84}Se observed in this work, with their spin-parity and their associated γ transitions. The values of the literature are taken from [23].

Level Energy (keV)		J^π	$J_i^\pi \rightarrow J_f^\pi$	E_γ (keV)	
This work	Literature			This work	Literature
1348.5(1)	1348.5(1)	2^+	$2^+ \rightarrow 0^+$	1348.5(1)	1348.3(1)
2287.1(2)	2286.61(15)	4^+	$4^+ \rightarrow 2^+$	938.6(1)	938.3(1)
2525.1(2)	2524.7(4)	**(4^+)***	$(4^+) \rightarrow 2^+$	1176.6(1)	1176.2
2933.2(3)	2933.0(9)	(5^+)	$(5^+) \rightarrow 4^+$	646.1(1)	646.0
3227.6(3)	3225(2)	(6^+)	$(6^+) \rightarrow 4^+$	940.5(1)	940(1)
			$(6^+) \rightarrow (5^+)$	**294.1(2)***	-
3947.9(5)*	-	**(7^+)***	**$(7^+) \rightarrow (6^+)$**	**720.3(2)***	-

Table 2: List of all the levels of ^{82}Ge observed in this work, with their spin-parity and their associated γ transitions. The values of the literature are taken from [23]. Text in bold font and with a star corresponds to a new transition or to changed spin-parity states from this work

Hwang *et al.* [8] is well populated in our experiment (we report an excitation energy of 2525.1(2) keV compatible with the one reported in references [8,9]). However, in contrast to the results by Hwang *et al.*, this state is seen to be populated directly by the fission process and decays solely to the 2^+ state at 1348.5 keV through the emission of a 1176.6 keV γ-ray, and not to the ground state. These two observations cast serious doubts on its previous 2^+ spin-parity assignment. It is important to mention that this state has also been observed to be populated by β-n decay of ^{83}Ga [25]. As in our case, the authors of Ref. [25] observed only one γ-decay channel from this state, to the 2^+ state at 1348.5 keV. While a state population depends on the reaction mechanism, its de-excitation process does not depend on the way it has been populated. As a consequence, three arguments bring us to reconsider the 2^+ spin-parity assignment made for the state at 2525.1 keV in ^{82}Ge:

- the absence of a direct decay branch to the ground state seems hardly compatible with a 2^+ spin-parity assignment;
- to our knowledge, this state has not been populated in the β-decay of ^{82}Ga while another 2^+ state at 2215.4 keV was well populated with an intensity $I_\beta = 17\%$ [25];
- as no feeding γ-transition is observed in our data, we can reasonably assume that this state is directly fed by the reaction with a relatively large probability ($I_\gamma = 22\%$). According to the current knowledge on spin population by fission, it is unlikely that this can happen for a 2^+ state located well above the yrast line.

In order to propose a spin assignment that is compatible with all these observations, we may use additional arguments from β-n selection rules. In the β-n decay of the ^{83}Ga $\frac{5}{2}^-$ ground state, states with angular momenta ranging from 0 to 5 $\hbar$ are populated, and positive parity is favored due to the dominant emission of $\ell = 1$ neutrons [25]. As the 2525.1 keV state decays to the 2^+ state at 1348.5 keV and not to the ground state, the range of possible spin-parity values for this state may be further restricted to $(3-4)^+$, of which the 4^+ hypothesis seems the most realistic considering the rather large energy of the transition from this state to the 2^+ state, 1176.6 keV, well compatible with an E2 character in this mass region. We therefore propose that the spin-parity of the state at 2525.1 keV in ^{82}Ge is 4^+ instead of 2^+. We note that this is well compatible with the shell model results presented in [9], where the 4_2^+ state appears at an excitation energy close to that observed here.

5.1.3 The new state at 3947.9 keV

This state is observed to decay solely to the (6^+) level at 3227.6 keV *via* a low-energy transition. Such low-energy transition is more likely to be of M1 type. We can thus assume that the spin of this excited state lies in the range $(5-7)^+$. Systematics arguments can help in further constraining this spin assignment : as can be seen in Figure 8 this state turns out to follow with an excellent agreement the trend of the 7^+ states of the heavier $N = 50$

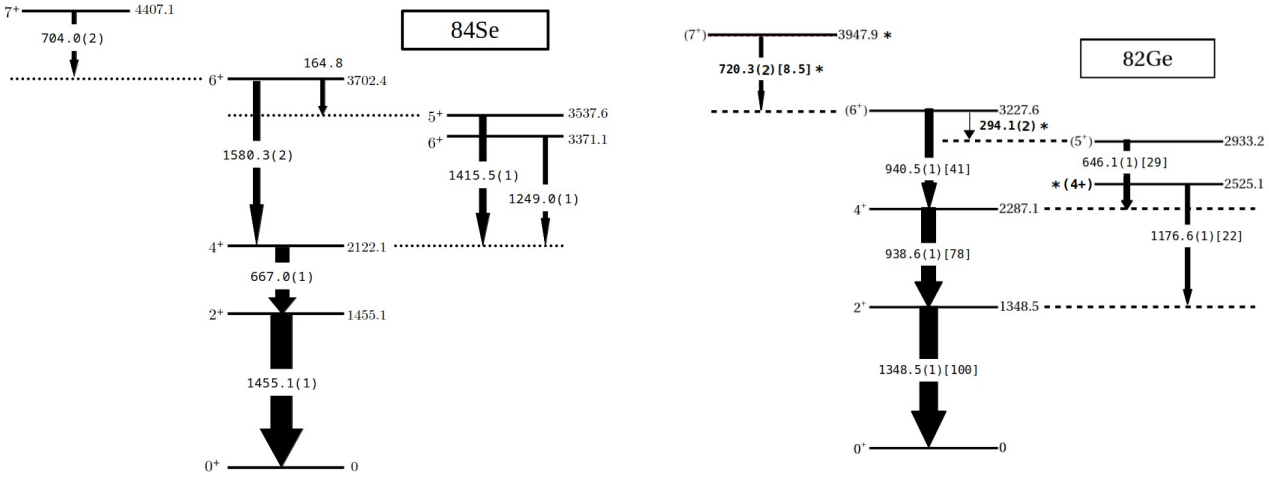

Fig. 7: On the left: Level scheme of ^{84}Se nucleus reconstructed from the data acquired during this experiment. All levels and transitions up to the (7^+) state at 4407.1 keV are seen in our experiment.
On the right: Level scheme of ^{82}Ge obtained from this work. New levels, transitions and spin assignments are indicated with an asterisk. Energies are given in keV. The transition intensities, given in square brackets, are relative to the $2^+ \rightarrow 0^+$ transition.

isotones. Moreover, it has a similar de-excitation pattern (see Figure 7) as the 7^+ state of the immediate even-even neighboring isotone. Thus, we propose a (7^+) spin-parity assignment to the 3947.9 keV excited state in ^{82}Ge.
As explained in the Introduction, a state with $J^\pi = 7^+$ in ^{82}Ge can only originate from a neutron core-breaking configuration. In the following section we discuss the consequence of the placement of this new energy state in the ^{82}Ge level scheme on our understating of the $N = 50$ major shell gap energy evolution along the isotonic line towards ^{78}Ni.

5.2 Evolution of the neutron shell gap in light $N = 50$ isotones from a spectroscopic point of view

5.2.1 Context

The occurrence of discontinuities in the derivatives of the mass surface, such as the systematics of neutron, proton or α separation energies, at magic numbers, were identified very early in the history of nuclear structure [27]. Soon after, Brueckner was able to relate the separation energy of a nucleon to an individual-particle energy within a shell model picture [28]. Since then, while it is clear that these mass surface derivatives at shell closures contain some information on the magnitude of the associated gap $\Delta\varepsilon$ between single-particle states, a quantitative extraction of $\Delta\varepsilon$ remains difficult and subject to discussion, especially far from double-shell closures. It is nevertheless of primary importance to be able to follow the trends of $\Delta\varepsilon$ along magic-number isotopic and isotonic chains because this quantity is a key ingredient of the evolution of the shell structure far from stability. In this respect, it is worth noting the interesting suggestion of Heyde *et al.* [26] which allows, by a graphical method, to get rid of the "upper shell effects" in the extraction of gaps from the systematics of the one-nucleon separation energies.

The evolution of the $N = 50$ shell gap as a function of the proton number, $\Delta\varepsilon^{[N=50]}(Z)$, from stability ($Z \approx 40$) down to $Z = 28$, has long been studied and discussed. A first model-dependent attempt to relate the magnitude of $\Delta\varepsilon^{[N=50]} = \varepsilon_{\nu d5/2} - \varepsilon_{\nu g9/2}$ to the excitation energy of some specific excited yrast (supposedly neutron-core breaking) states of light $N = 50$ isotones is due to Zhang *et al.* [5]. Sahin *et al.* [9] completed this work some time later, and they arrived at an estimate of the effective $N = 50$ energy gap of $\Delta\varepsilon^{[N=50]} = \varepsilon_{\nu d5/2} - \varepsilon_{\nu g9/2} = 3.6$ MeV at $Z = 32$. Almost simultaneously, Porquet and Sorlin [29], expecting a linear evolution of $\Delta\varepsilon^{[N=50]}(Z)$ as Z decreases, discussed in detail the fact that the one-neutron separation energy (S_n) of ^{83}Ge deviated significantly from a linear trend. They concluded, using a complex network of binding energy data, that $\Delta\varepsilon^{[N=50]}(Z)$ is reduced by 0.55 MeV between $Z = 38$ and $Z = 28$. Finally, Verney showed [11] that using the method of Ref. [26] to extract $\Delta\varepsilon^{[N=50]}(Z) = \varepsilon_{\nu d5/2} - \varepsilon_{\nu g9/2}$, one indeed obtains a quasi-linear trend with Z, and, even more interesting, that the $\Delta\varepsilon^{[N=50]}(Z)$ curve overlaps practically exactly with the 6_1^+ energy systematics of the light even-even $N = 50$ isotones. In the following section, we explore the reasons for this remarkable agreement. The determination of the exact energy location of the 7^+ state in ^{82}Ge (a state even less subject to configuration mixing and correlations than the 6^+), achieved for the first time from the present work, is particularly interesting in this context.

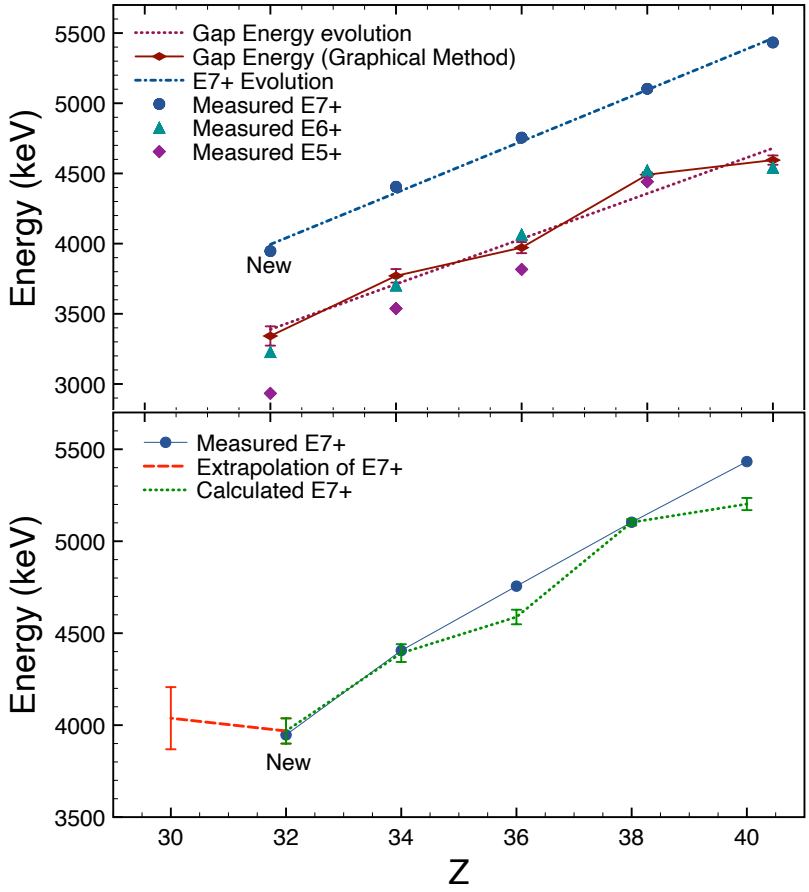

Fig. 8: Top panel: Evolution of the size of the gap $N = 50$ deduced from the graphical method of Ref. [26] for several even-even isotones. The systematics of the $1p$-$1h$ 5^+, 6^+, and 7^+ states are also shown. The error bars are smaller than the chosen icons. For comparison, the linear trends of the shell gap energy evolution and of the 7^+ energy evolution are shown with dashed lines. See text for details.
Bottom panel: Comparison between the calculated using equation 3 (dashed line) and experimentally measured (plain line) energy of the 7^+ state for several even-even $N = 50$ isotones. An extrapolation to ^{80}Zn is proposed.

5.2.2 On the nature of the ^{82}Ge 7^+ excited state

As remarked earlier, in a shell-model picture and to some approximation [28], an empirical value of the gap energy amplitude $\Delta\varepsilon^{[N=50]}(Z) = \varepsilon_{\nu d5/2} - \varepsilon_{\nu g9/2}$ can be obtained from the difference between neutron-separation energy values :

$$\begin{aligned}\Delta\varepsilon^{[N=50]}(Z) =& \varepsilon_{\nu d5/2} - \varepsilon_{\nu g9/2} \\ \approx& S_n(N=51) - S_n(N=50) \equiv \Delta S_n(Z)\end{aligned}$$

for even Z nuclei. As illustrated in Panel C of Figure 9, this S_n difference involves the binding energies (BE) of three nuclei in their ground states. Following Ref. [30] one may decompose the energy content of the shell-model configurations involved, as shown in the same picture. If good shell closures are present at $Z = 28$ and $N = 50$, the only pairing energy terms originate from the proton fp open shell and cancel out in the S_n difference. It results that :

$$\begin{aligned}\Delta S_n(Z) =& \varepsilon_{\nu d5/2} - \varepsilon_{\nu g9/2} \\ &+ V_{[\pi_0 \nu d_{5/2}]_{5/2^+}} + V_{[\pi_0 (\nu g_{9/2})^{-1}]_{9/2^+}}\end{aligned} \quad (1)$$

where $V_{[\pi_0 \nu d_{5/2}]_{5/2^+}}$ and $V_{[\pi_0 (\nu g_{9/2})^{-1}]_{9/2^+}}$ represent the interaction energy between the single $\nu d_{5/2}$ particle and $\nu g_{9/2}$ hole and the $(N = 50, J = 0^+)$ ground state, respectively. One may now compare this energy content to the one of a pure neutron-core breaking, particle-hole configuration $(\nu\nu^{-1} = d_{5/2} g_{9/2}^{-1})$ coupled to a given total angular momentum $J_{\nu\nu^{-1}}$. This decomposition is shown graphically in Panel B of Figure 9. The excitation energy of this pure configuration then reads :

$$\begin{aligned}E^*(J_{\nu\nu^{-1}}) =& \varepsilon_{\nu d5/2} - \varepsilon_{\nu g9/2} \\ &+ V_{[\pi_0 \nu d_{5/2}]} + V_{[\pi_0 \nu g_{9/2}]} + V_{[\nu d_{5/2} \nu g_{9/2}]_{J_{\nu\nu^{-1}}}}\end{aligned} \quad (2)$$

where $V_{[\nu d_{5/2} \nu g_{9/2}]_{J_{\nu\nu^{-1}}}}$ is the particle-hole interaction energy in channel $J_{\nu\nu^{-1}}$. Combining equations (1) and (2)

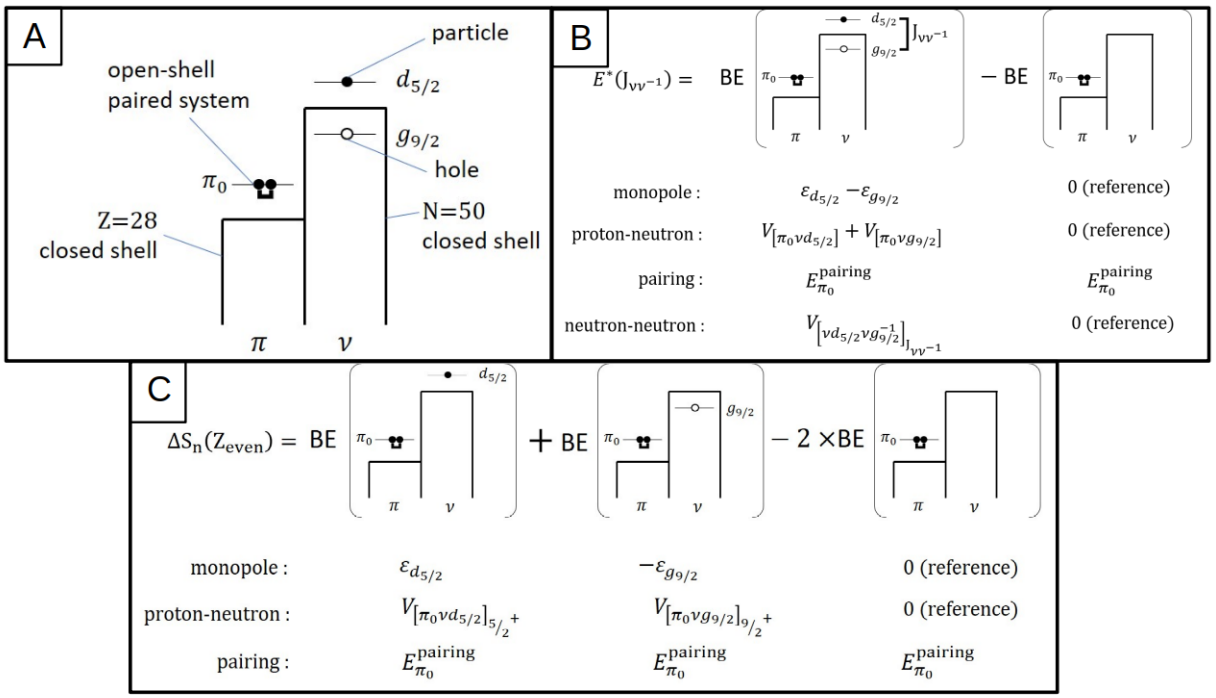

Fig. 9: Panel A : legend explaining the meaning of the graphs used in other Panels. Panel B : energy decomposition of a core-breaking particle-hole $\nu\nu^{-1}$ state of total angular momentum $J_{\nu\nu^{-1}}$ along the single-particle "mean field" (called here monopole), proton-neutron, pairing, and neutron-particle neutron-hole (called here neutron-neutron) components. Panel C : Same as Panel B but for the ΔS_n gap expression (see text for more details).

one sees that the two expressions differ essentially by this last term. If one considers the $V_{[\pi_0 \nu_j]}$ terms as being of monopole nature, they can be included into an effective single particle energy $\tilde{\varepsilon}(Z)$. In such conditions, for the pure particle-hole configuration $(g_{9/2})^{-1}(d_{5/2})^1$, the energy of the corresponding 7^+ state takes the form:

$$E(g^{-1}_{9/2}d^1_{5/2}; 7^+) = \tilde{\varepsilon}_{d_{5/2}} - \tilde{\varepsilon}_{g_{9/2}} + \left\langle g^{-1}_{9/2}d^1_{5/2}\middle|V_{12}\middle|g^{-1}_{9/2}d^1_{5/2}\right\rangle_{J=7^+}$$

where $\left\langle g^{-1}_{9/2}d^1_{5/2}\middle|V_{12}\middle|g^{-1}_{9/2}d^1_{5/2}\right\rangle_{J=7^+}$ can be considered as the two-body matrix element of a valence residual interaction. Such matrix elements, which connect two natural neutron valence spaces below and above the $N = 50$ shell closure, are not easily found in literature. In a first crude approach, and in order to verify our hypothesis, we may rely on a simple schematic interaction like a δ contact-interaction. If one uses the following form :

$$V_{12} = -V_0\delta(\mathbf{r_1} - \mathbf{r_2})$$

the two-body matrix element then reads:

$$\langle j_1 j_2|V_{12}|j_1 j_2\rangle_J = -V_0 \times F_R(n_1 n_2 \ell_1 \ell_2) \times A(j_1 j_2 J)$$

with V_0, the depth of a Woods-Saxon potential, $F_R(n_1 n_2 \ell_1 \ell_2)$, the overlap integral between the wave-functions of the two single particle orbitals, and $A(j_1 j_2 J)$, a geometric term involving only the angular quantum numbers of the system. The strength of the δ-interaction is empirically determined from the observed energy splitting of the $(g_{9/2})^{-1}(d_{5/2})^1$ particle-hole multiplet members identified in the stable $N = 50$ isotone ^{88}Sr, after Pandya particle-hole to particle-particle transformation [31]. Since we are only interested in the energy evolution of the 7^+ member of this multiplet, $E(g^{-1}_{9/2}d^1_{5/2}; 7^+)$, as a function of Z, or equivalently A, for even-even $N = 50$ isotones, it is sufficient to rearrange this expression into the following form, showing the Z or A dependence explicitly:

$$E(g^{-1}_{9/2}d^1_{5/2}; 7^+) = \Delta\tilde{\varepsilon}^{[N=50]}(Z) + \frac{\text{const}}{A^{1/3}} \qquad (3)$$

In this expression the energy gap amplitude as a function of Z, $\Delta\tilde{\varepsilon}^{[N=50]}(Z)$, is taken from available mass data [32] following the prescription of Ref. [26] similarly as in Ref. [11]. It is shown graphically in Figure 8 (upper panel). The constant term contains the δ-interaction strength extracted as just explained. The 7^+ state excitation energy values obtained are also reported in Figure 8 (bottom panel). As can be seen, the calculated energies using our simple model reproduce the experimental ones down to $^{82}_{32}$Ge with a precision ranging from 20 keV to 100 keV. We obtain $E(g^{-1}_{9/2}d^1_{5/2}; 7^+) = 3968(86)$ keV at $Z = 32$, in almost perfect agreement with the 7^+ excitation energy value of 3947.9 keV observed in our experiment. This agreement is certainly partially accidental as it cannot be

expected from a model where configuration mixing is neglected. However it is remarkable that the energy trend remains accurate as far as 6 mass units from the reference nucleus, showing that the essential physics ingredients driving this evolution are captured in this simple picture. This analysis also further supports our attribution of a spin-parity of 7^+ for the new state at 3947.9 keV, whose structure can be assigned to the neutron-core breaking $(g_{9/2})^{-1}(d_{5/2})^1$ configuration.

As can be seen in the top panel of Figure 8 the similarity in the evolution with Z of the 7^+ and 6^+ energies with that of $N = 50$ shell gap energy is a striking feature of this mass region. The slopes of these linear trends are 161 keV/A for the gap, 183 keV/A for the 7^+ state, and 172 keV/A for the 6^+ state. The gap slope is almost three times as high as the one obtained in Ref. [29]. We obtain an effective gap value of 3320(76) keV at $Z = 32$, a value close but even lower than the one obtained in Ref. [9]. Our results therefore definitely support a rather strong reduction of the effective $N = 50$ gap, from $Z = 38$ down to $Z = 32$, stronger than discussed previously.

Finally, it is worth noting that 5^+ states energies drop faster than those of the 6^+ and 7^+ states when one removes protons, as the measured slope is 240.1 keV/A. This feature is actually consistent with the known single particle structure in this region. It is well known that the $\nu 3s_{1/2}$ orbital is getting closer to the $\nu 2d_{5/2}$ when one removes protons from $N = 50$ nuclei. This migration has been explained by Delafosse *et al.* [33] as an effect of the isospin asymmetry of the pseudo-spin symmetry in this region. As a consequence, the configuration $(\nu 1g_{9/2})^{-1}(\nu 3s_{1/2})^1$ must also enter into the composition of the 5^+ wave function in the lightest $N = 50$ isotones. This configuration generates a 4^+ and a 5^+ state which will mix with the equal spin states generated by the $(g_{9/2})^{-1}(d_{5/2})^1$ configuration. This would naturally explain a faster drop in energy of the $(5_1{}^+)$ state. This effect should not change the (6^+) and (7^+) energies, which is consistent with our observations.

6 Conclusion

In this work, yrast and near-yrast states of the neutron-rich nucleus ^{82}Ge were successfully populated using the fast neutron-induced fission of ^{232}Th. Due to the performance of the ν-Ball spectrometer, using triple γ-coincidences, two previously unreported transitions could be firmly assigned to ^{82}Ge. These transitions were placed in the level scheme and a new level was introduced at 3947.9 keV excitation energy. We assign this new state to $J^\pi = 7^+$ originating from the neutron-core breaking particle-hole configuration $(\nu 1g_{9/2})^{-1}(\nu 2d_{5/2})^1$. This new information was used to quantify the evolution of the $N = 50$ gap from $Z = 38$ down to $Z = 32$. According to our analysis, the gap slope is almost three times as high as the one obtained in Ref. [29], and the effective gap value of 3320(76) keV at $Z = 32$ is obtained and is consistent, but even lower, than that reported in Ref. [9]. This is coherent with the observed strong reduction of the effective $N = 50$ gap, from $Z = 38$ down to $Z = 32$, but this reduction seems greater than has been discussed previously. Our model also allows us to propose an estimate for the position of the 7^+ state in ^{80}Zn which we predict will be located around 4008(169) keV excitation energy (see Figure 8). Future direct measurements of the energy of this state, and those of other members of the state multiplet generated by the $(\nu 1g_{9/2})^{-1}(\nu 2d_{5/2})^1$ configuration would provide crucial information to better understand the peculiar neutron-shell structure evolution towards ^{78}Ni.

7 Acknowledgments

We would like to thank the operators of the ALTO facility for providing us with reliable beams used in the experiments. We would like to express our profound gratitude to the FASTER collaboration for their strong technical support over the course of the campaign. We would like to acknowledge the support of the GAMMA-POOL and the LOANPOOL for the loan of the Clovers and Phase I germanium detectors. We also acknowledge the FATIMA collaboration for the loan of their $LaBr_3$ crystals. G. Häfner and R. Lozeva acknowledge support from the IDEX-API grant. A. Blazhev, R.-B. Gerst and N. Warr are supported by the DFG under Grant No.BL 1513/1-1. The research leading to these results has received funding from the European Union's HORIZON2020 Program under grant agreement No.654002. P.-A. Söderström, P. Koseoglou, J. Wiederhold, M. Rudigier, C. Henrich, I. Homm, C. Sürder and T. Kröll acknowledge the support from BMBF in Germany under grant NuSTAR.DA 05P15RDFN1. P.-A. Söderström acknowledges the contract PN 23 21 01 06 sponsored by the Romanian Ministry of Research, Innovation and Digitalization. A. Korgul acknowledges the Polish National Science Center under Grant No.2020/39/B/ST2/02346 that partially funded this work. L. Iskra acknolegdes the Polish National Science Centre, Poland, under research project No.2020/39/D/ST2/03510. This work is partially supported via the UK STFC UK Nuclear Data Network, UK STFC (grants ST/G000697/1, ST/P005314, ST/P003982/1 and ST/L005743/1) (PHR) and the University of Surrey Marion Redfearn Trust (RCL). P.-H. Regan, M. Bunce, A. Boso and P. Ivanov acknowledge support from the UK Department of Business, Energy and Industrial Strategy (BEIS) via the National Measurement System.

References

1. Ch. Engelmann, F. Ameil, P. Armbruster, M. Bernas, S. Czajkowski, Ph. Dessagne, C. Donzaud, H. Geissel, A. Heinz, Z. Janas, C. Kozhuharov, Ch. Miehe, G. Munzenberg, M. Pfutzner, C. Rohl, W. Schwab, C. Stephan, K. Summerer, L. Tassan-Got, and B. Voss. *Production and Identification of Heavy Ni Isotopes: Evidence for the doubly magic nucleus $^{78}_{28}$Ni. Z.Phys.*, A352:351, 1995.
2. R. Taniuchi, C. Santamaria, P. Doornenbal, A. Obertelli, K. Yoneda, G. Authelet, H. Baba, D. Calvet, F. Château, A. Corsi, A. Delbart, J.-M. Gheller, A. Gillibert, J. D.

Holt, T. Isobe, V. Lapoux, M. Matsushita, J. Menéndez, S. Momiyama, T. Motobayashi, M. Niikura, F. Nowacki, K. Ogata, H. Otsu, T. Otsuka, C. Péron, S. Péru, A. Peyaud, E. C. Pollacco, A. Poves, J.-Y. Roussé, H. Sakurai, A. Schwenk, Y. Shiga, J. Simonis, S. R. Stroberg, S. Takeuchi, Y. Tsunoda, T. Uesaka, H. Wang, F. Browne, L. X. Chung, Z. Dombradi, S. Franchoo, F. Giacoppo, A. Gottardo, K. Hadyńska-Klęk, Z. Korkulu, S. Koyama, Y. Kubota, J. Lee, M. Lettmann, C. Louchart, R. Lozeva, K. Matsui, T. Miyazaki, S. Nishimura, L. Olivier, S. Ota, Z. Patel, E. Şahin, C. Shand, P.-A. Söderström, I. Stefan, D. Steppenbeck, T. Sumikama, D. Suzuki, Z. Vajta, V. Werner, J. Wu, and Z. Y. Xu. *^{78}Ni revealed as a doubly magic stronghold against nuclear deformation. Nature*, 569(7754):53–58, May 2019.

3. J. Hakala, S. Rahaman, V.-V. Elomaa, T. Eronen, U. Hager, A. Jokinen, A. Kankainen, I. D. Moore, H. Penttilä, S. Rinta-Antila, J. Rissanen, A. Saastamoinen, T. Sonoda, C. Weber, and J. Äystö. *Evolution of the N=50 Shell Gap Energy towards* ^{78}Ni. *Phys. Rev. Lett.*, 101:052502, Jul 2008.
4. S. Baruah, G. Audi, K. Blaum, M. Dworschak, S. George, C. Guénaut, U. Hager, F. Herfurth, A. Herlert, A. Kellerbauer, H.-J. Kluge, D. Lunney, H. Schatz, L. Schweikhard, and C. Yazidjian. *Mass Measurements beyond the Major r-Process Waiting Point* ^{80}Zn. *Phys. Rev. Lett.*, 101:262501, Dec 2008.
5. Y. H. Zhang, Zs. Podolyàk, G. de Angelis, A. Gadea, C. Ur, S. Lunardi, N. Marginean, C. Rusu, R. Schwengner, Th. Kröll, D. R. Napoli, R. Menegazzo, D. Bazzacco, E. Farnea, S. Lenzi, T. Martinez, M. Axiotis, D. Tonev, W. Gelletly, S. Langdown, P. H. Regan, J. J. Valiente Dobon, W. von Oertzen, B. Rubio, B. Quintana, N. Medina, R. Broda, D. Bucurescu, M. Ionescu-Bujor, and A. Iordachescu. *Stability of the* N=50 *shell gap in the neutron-rich* Rb*,* Br*,* Se*, and* Ge *isotones. Phys. Rev. C*, 70:024301, Aug 2004.
6. A. Prévost, A. Astier, I. Deloncle, M.-G. Porquet, F. Azaiez, A. Buta, D. Curien, O. Dorvaux, G. Duchêne, B. J. P. Gall, F. Khalfallah, I. Piqueras, M. Rousseau, F. Ibrahim, S. Essabaa, M. Meyer, N. Redon, O. Stézowski, Ts. Venkova, R. Lucas, and A. Bogachev. *In-Beam γ-Ray Spectroscopy of the* N=50 *Isotones on the Neutron-Rich Side. AIP Conference Proceedings*, 802(1):279–282, 2005.
7. T. Rząca-Urban, W. Urban, J. L. Durell, A. G. Smith, and I. Ahmad. *New excited states in* ^{82}Ge*: Possible weakening of the $N = 50$ closed shell. Phys. Rev. C*, 76:027302, Aug 2007.
8. J. K. Hwang, J. H. Hamilton, A. V. Ramayya, N. T. Brewer, Y. X. Luo, J. O. Rasmussen, and S. J. Zhu. *Possible excited deformed rotational bands in* ^{82}*Ge. Phys. Rev. C*, 84:024305, Aug 2011.
9. E. Sahin, G. de Angelis, G. Duchene, T. Faul, A. Gadea, A.F. Lisetskiy, D. Ackermann, A. Algora, S. Aydin, F. Azaiez, D. Bazzacco, G. Benzoni, M. Bostan, T. Byrski, I. Celikovic, R. Chapman, L. Corradi, S. Courtin, D. Curien, U. Datta Pramanik, F. Didierjean, O. Dorvaux, M.N. Erduran, S. Erturk, E. Farnea, E. Fioretto, G. de France, S. Franchoo, B. Gall, A. Gottardo, B. Guiot, F. Haas, F. Ibrahim, E. Ince, A. Khouaja, A. Kusoglu, G. La Rana, M. Labiche, D. Lebhertz, S. Lenzi, S. Leoni, S. Lunardi, P. Mason, D. Mengoni, C. Michelagnoli, V. Modamio, G. Montagnoli, D. Montanari, R. Moro, B. Mouginot, D.R. Napoli, D. O'Donnell, J.R.B. Oliveira, J. Ollier, R. Orlandi, G. Pollarolo, F. Recchia, J. Robin, M.-D. Salsac, F. Scarlassara, R.P. Singh, R. Silvestri, J.F. Smith, I. Stefan, A.M. Stefanini, K. Subotic, S. Szilner, D. Tonev, D.A. Torres, M. Trotta, P. Ujic, C. Ur, J.J. Valiente-Dobón, D. Verney, M. Yalcinkaya, P.T. Wady, K.T. Wiedemann, and K. Zuber. Structure of the *N=50 As, Ge, Ga* nuclei. *Nuclear Physics A*, 893:1–12, 2012.
10. J. Dudouet, A. Lemasson, G. Maquart, F. Nowacki, D. Verney, M. Rejmund, G. Duchêne, O. Stezowski, E. Clément, C. Michelagnoli, A. Korichi, C. Andreoiu, A. Astier, G. de Angelis, G. de France, C. Delafosse, I. Deloncle, F. Didierjean, Z. Dombradi, C. Ducoin, A. Gadea, A. Gottardo, D. Guinet, B. Jacquot, P. Jones, T. Konstantinopoulos, I. Kuti, F. Le Blanc, S. M. Lenzi, G. Li, R. Lozeva, B. Million, D. R. Napoli, A. Navin, R. M. Pérez-Vidal, C. M. Petrache, D. Ralet, M. Ramdhane, N. Redon, C. Schmitt, and D. Sohler. Excitations of the magic *N=50* neutron-core revealed in ^{81}Ga. *Phys. Rev. C*, 100:011301, Jul 2019.
11. D. Verney. Etude de l'effet de couche N=50 en direction de ^{78}Ni: contribution des études de radioactivité auprès du séparateur en ligne PARRNe. Manuscript de *HDR*, Institut de Physique Nucléaire d'Orsay, Université Paris-Sud XI, 2013.
12. S. Leoni, C. Michelagnoli, and J. N. Wilson. *Gamma-ray spectroscopy of fission fragments with state-of-the-art techniques. La Rivisita del Nuovo Cimento*, 45:461–547, 2022.
13. M. Lebois, N. Jovančević, D. Thisse, R. Canavan, D. Etasse, M. Rudigier, and J.N. Wilson. *The ν-ball γ-spectrometer. Nuclear Instruments and Methods in Physics Research Section A: Accelerators, Spectrometers, Detectors and Associated Equipment*, 960:163580, 2020.
14. M. Lebois, N. Jovančević, J.N. Wilson, D. Thisse, R. Canavan, and M. Rudigier. *The ν-ball Campaign at ALTO. Acta Physica Polonica B*, 50:425, 2019.
15. *GAMMAPOOL.* `http://gammapool.lnl.infn.it/index.html`, Accessed: June 1, 2023.
16. *LOANPOOL.* `http://ipnwww.in2p3.fr/GePool/poolRules.html`, Accessed: June 1, 2023.
17. Oliver J. Roberts, Alison M. Bruce, Patrick H. Regan, Zsolt Podolyák, Christopher M. Townsley, John F. Smith, Kieran F. Mulholland, and Andrew Smith. *A LaBr3: Ce fast-timing array for DESPEC at FAIR. Nuclear Instruments and Methods in Physics Research Section A: Accelerators, Spectrometers, Detectors and Associated Equipment*, 748:91–95, 2014.
18. *UKNDN.* `http://www.ukndn.ac.uk`, Accessed: June 1, 2023.
19. *Fast Acquisition System for nuclEar Research.* `http://faster.in2p3.fr/`, Accessed: June 1, 2023.
20. M. Lebois, J.N. Wilson, P. Halipré, B. Leniau, I. Matea, A. Oberstedt, S. Oberstedt, and D. Verney. *Development of a kinematically focused neutron source with the p(^{7}Li,n)^{7}Be inverse reaction. Nuclear Instruments and Methods in Physics Research Section A: Accelerators, Spectrometers, Detectors and Associated Equipment*, 735:145–151, 2014.
21. *JENDL FP Fission Yields Data File 2011.* `https://wwwndc.jaea.go.jp/cgi-bin/FPYfig`, Accessed: June 1, 2023.

22. D. Thisse. *Étude des états particule-trou dans les noyaux de la région du ^{78}Ni avec le spectromètre ν-Ball. Thèse de doctorat de l'Université Paris-Saclay*, 2021.
23. J. K. Tuli and E. Browne. *Data extracted using the* NNDC *On-Line Data Service from the* ENSDF *database, file revised as of March 2019. NDS*, 157:260, 2019.
24. P. Hoff and B. Fogelberg. *Properties of strongly neutron-rich isotopes of germanium and arsenic. Nuclear Physics A*, 368(2):210–236, 1981.
25. D. Verney, D. Testov, F. Ibrahim, Yu. Penionzhkevich, B. Roussière, V. Smirnov, F. Didierjean, K. Flanagan, S. Franchoo, E. Kuznetsova, R. Li, B. Marsh, I. Matea, H. Pai, E. Sokol, I. Stefan, and D. Suzuki. *Pygmy Gamow-Teller resonance in the $N = 50$ region: New evidence from staggering of β-delayed neutron-emission probabilities. Phys. Rev. C*, 95:054320, May 2017.
26. K. Heyde, J. Jolie, J. Moreau, J. Ryckebusch, M. Waroquier, and J.L. Wood. *A new prescription for determining particle-hole interactions near closed shells. Physics Letters B*, 176(3):255–259, 1986.
27. E. Glueckauf. *Some Observations concerning the Energy of Nuclei. Proc. Phys. Soc.*, 61:25–33, 1947.
28. Keith A. Brueckner. *Single-Particle Energy and Effective Mass and the Binding Energy of Many-Body Systems. Phys. Rev.*, 110:597–600, May 1958.
29. M.-G. Porquet and O. Sorlin. *Evolution of the $N = 50$ gap from $Z = 30$ to $Z = 38$ and extrapolation toward ^{78}Ni. Phys. Rev. C*, 85:014307, Jan 2012.
30. Nissan Zeldes. *Nuclear energies and the shell model. Nuclear Physics*, 7:27–110, 1958.
31. Sudhir P. Pandya. *Nucleon-Hole Interaction in* jj *Coupling. Phys. Rev.*, 103:956–957, Aug 1956.
32. W.J. Huang, G. Audi, Meng Wang, F. G. Kondev, S. Naimi, and Xing Xu. *The AME2016 atomic mass evaluation (I). Evaluation of input data; and adjustment procedures. Chinese Physics C*, 41(3):030002, mar 2017.
33. C. Delafosse, D. Verney, P. Marević, A. Gottardo, C. Michelagnoli, A. Lemasson, A. Goasduff, J. Ljungvall, E. Clément, A. Korichi, G. De Angelis, C. Andreoiu, M. Babo, A. Boso, F. Didierjean, J. Dudouet, S. Franchoo, A. Gadea, G. Georgiev, F. Ibrahim, B. Jacquot, T. Konstantinopoulos, S. M. Lenzi, G. Maquart, I. Matea, D. Mengoni, D. R. Napoli, T. Nikšić, L. Olivier, R. M. Pérez-Vidal, C. Portail, F. Recchia, N. Redon, M. Siciliano, I. Stefan, O. Stezowski, D. Vretenar, M. Zielinska, D. Barrientos, G. Benzoni, B. Birkenbach, A. J. Boston, H. C. Boston, B. Cederwall, L. Charles, M. Ciemala, J. Collado, D. M. Cullen, P. Désesquelles, G. de France, C. Domingo-Pardo, J. Eberth, V. González, L. J. Harkness-Brennan, H. Hess, D. S. Judson, A. Jungclaus, W. Korten, A. Lefevre, F. Legruel, R. Menegazzo, B. Million, J. Nyberg, B. Quintana, D. Ralet, P. Reiter, F. Saillant, E. Sanchis, Ch. Theisen, and J. J. Valiente Dobon. *Pseudospin Symmetry and Microscopic Origin of Shape Coexistence in the ^{78}Ni Region: A Hint from Lifetime Measurements. Phys. Rev. Lett.*, 121:192502, Nov 2018.